Heliyon 10 (2024) e37257

Contents lists available at ScienceDirect

Heliyon

journal homepage: www.cell.com/heliyon

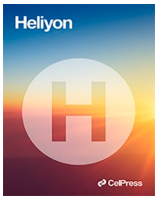

Research article

Pharmacodynamics of Sishen decoction in relieving rheumatoid arthritis: Chemical composition, regulatory pathway and online prediction simulation

Mengyao Gao [a,b], Jun Liu [b], Quansheng Li [c], Yeyu Zhao [a], Xin Jin [b], Xinyi Tang [a], Congxi Li [a], Mingli Gao [a,b,*]

[a] Liaoning University of Traditional Chinese Medicine, China
[b] Affiliated Hospital of Liaoning University of Traditional Chinese Medicine, Shenyang, China
[c] Department of Allergy, Shengjing Hospital of China Medical University, Shenyang, China

ARTICLE INFO

Keywords:
Sishen decoction
Rheumatoid arthritis
Chemical composition
PI3K/AKT pathway
Computational simulation

ABSTRACT

As a commonly used traditional Chinese medicine formula for treating rheumatoid arthritis (RA), Sishen Decoction (SSD) has anti-inflammatory, analgesic and swelling relief effects. However, at present, the pharmacodynamic basis of SSD and its mechanism of treating RA have not been clarified, and further research is needed. Analyzing the pharmacological basis of SSD was the aim of our study and further elucidate its therapeutic mechanism and potential targets for treating RA. LC–MS was used to identify the high content and characteristic chemical components of SSD. On this basis, a network of pharmacological analysis was established between the chemical structure and RA. According to the predicted possible pathways and targets, *in vivo* pharmacodynamic experiments and related pathway analysis were conducted. Finally, the possible targets and mechanisms of SSD in treating RA were analyzed. Identified 78 compounds from SSD by LC-MS, including 23 flavonoids, 19 phenolic acids, 9 monoterpenoids and 26 other compounds. Network pharmacological analysis based on pharmacodynamic substances revealed that the most likely interaction pathway between SSD and RA was the PI3K/AKT/mTOR pathway. Foot swelling and inflammatory factors (IL-6, IL-10, IL-18, TGF, TNF-α, VEGF) in model mice were shown to be significantly improved *in vivo*. WB and qPCR experiments proved that SSD could significantly regulate the pathway of PI3K/AKT/mTOR. The interaction between SSD and AKT target was further analyzed by multispectroscopy. This study revealed that SSD alleviates RA by regulating the pathway of PI3K/AKT/mTOR and preliminarily revealed the pharmacodynamic mechanism of SSD for the first time.

1. Introduction

Rheumatoid arthritis (RA), a persistent autoimmune disorder characterized by inflammation, typically manifests as a balanced attack on small joints across the body, including those in the hands and feet. Epidemiological surveys have shown that worldwide, the prevalence rate for women and men is 3:1, with a total incidence rate ranging from 0.4 % to 1.3 %. Data show that RA is more common

* Corresponding author. Liaoning University of Traditional Chinese Medicine, China.
E-mail address: gmllnzy@163.com (M. Gao).

https://doi.org/10.1016/j.heliyon.2024.e37257
Received 1 February 2024; Received in revised form 18 August 2024; Accepted 29 August 2024
Available online 30 August 2024
2405-8440/© 2024 Published by Elsevier Ltd. This is an open access article under the CC BY-NC-ND license (http://creativecommons.org/licenses/by-nc-nd/4.0/).

in elderly people aged 65–74 years, and there are regional differences [1]. The characteristic pathological changes of RA mainly include synovial hyperplasia, pannus formation, and bone and cartilage damage [2]. In the early stage of RA, the main symptoms are recurrent and persistent synovial hyperplasia and the formation of pannus. As the disease progresses, irreversible bone and cartilage damage occurs, leading to varying degrees of joint damage, limb deformities, and even disability [3]. Due to the pathological characteristics of multiple mechanisms and factors involved in the development of RA, it often leads to the occurrence of cardiovascular and other systemic complications, even leading to death in severe cases. Researchers are studying this type of rheumatoid arthritis because it wreaks havoc on patients' quality of life and survival rates, but its pathogenic factors have not been fully elucidated [4,5]. Currently, no specific drugs have been developed to cure RA. In clinical treatment, the current treatment principle is still early diagnosis, symptom relief, delayed disease progression, and improved limb function [6].

At present, the treatment of rheumatoid arthritis employs several types of medications including non-steroidal anti-inflammatory drugs (NSAIDs), disease-modifying anti-rheumatic drugs (DMARDs), and immunosuppressive glucocorticoids (GCs) [7]. The main effects of the first two types of drugs are to alleviate clinical symptoms caused by inflammation (such as pain and joint swelling) and reduce synovitis and systemic inflammatory reactions, thus achieving the goals of delaying joint damage and improving affected joint function. Among traditional RA drugs, the most commonly used is methotrexate (MTX). Low doses of MTX can inhibit RA inflammation by inhibiting the proliferation of inflammatory cells. It has been used as a first-line drug for early RA treatment for the past two decades. Although MTX can inhibit synovial inflammation (especially early synovitis), it cannot protect and repair the bone and cartilage tissue of the affected joint. Therefore, it is necessary to find new treatments that induce disease relief through permanent immune tolerance, protect normal tissue structure, minimize tissue damage, and repair existing damage [8,9].

Over the past few years, developed nations across the globe have increasingly adopted traditional Chinese medicine (TCM) as a means to both prevent and manage numerous chronic ailments. The use of TCM therapy for treating RA has become a research trend in the past several years. Many clinical studies proved that TCM therapy is reliable and can be used as an auxiliary treatment in combination with other therapies for treating RA [10,11]. It has a significant effect on shortening the course of medication, reducing medication dosage, and reducing the toxic side effects of medicine treatment. The Sishen Decotion (SSD) is derived from the "New Compilation of Experimental Prescriptions" written by Bao Xiangyi in the Qing Dynasty. In clinical settings, Traditional Chinese Medicine (TCM) has been practically applied to manage rheumatoid arthritis (RA). A significant research study by Li et al. evaluated the efficacy of Sishen decoction in treating RA [12]. Sixty-eight patients diagnosed with RA were enrolled and allocated into two groups: the observation group and the control group, each consisting of 34 patients. SSD can significantly reduce inflammatory indicators, relieve pain, and improve knee joint function. Wang et al. divided patients after arthroscopic cleaning of osteoarthritis tissue into a treatments and a controls, each group contained 18 patients [13]. The individuals in the experimental group received SSD, while those in the control group were administered capsules containing naphthalene bumethone. The results proved that the improvement of joint swelling, range of motion and tenderness in the treatments was significantly better than that in the controls. The combinations of *Astragalus membranaceus*, *Polygala tenuifolia*, *Achyranthes bidentata*, *Dendrobium nobile* and *Lonicera japonica* in the decotion have been reported to improve RA [14,15].

Traditional research methods are insufficient to explain the various chemical components, targets and pharmacological mechanisms of TCM [16]. Nevertheless, TCM can be understood through the lens of network pharmacology, an approach that merges bioinformatics with pharmacology. This methodology provides a systematic way to study the complex relationships among diseases, genes, targets, and medications. By developing a multi-layered network that maps out 'disease-target-drug' interactions and analyzing these connections, researchers can comprehensively predict and validate the effects of TCM. This allows for a deeper insight into how medications regulate disease processes at the levels of proteins, molecules, and genes [17,18].

This research primarily utilizes network pharmacology and molecular docking techniques to forecast and scrutinize the principal active ingredients, essential targets, and pivotal pathways in SSD treatments for RA. Furthermore, used LC–MS to analyze the main compound composition, and animal models were used to explore the actual intervention effect *in vivo*. The mechanism of SSD in treating RA was deeply analyzed from two dimensions, predictive analysis and experimental analysis, laying a theoretical foundation for its use in clinical settings.

2. Materials and methods

2.1. Chemicals and reagents

The doses of SSD used in this study were *Astragalus membranaceus* (rhizome, 240 g), *Dendrobium nobile* (stem barks, 120 g), *Polygala tenuifolia* (roots, 90 g), *Achyranthes bidentata* (rhizome, 90 g), and *Lonicera japonica* (flowers, 30 g). The pharmaceuticals originated from the First Affiliated Hospital of Liaoning University of Traditional Chinese Medicine's Preparation Center, where they were formulated into a liquid. High-purity reagents used in the mass spectrometry included methanol, acetonitrile, ammonium acetate, and ethanoic acid, all sourced from Merck in Darmstadt, Germany. Additionally, the deionized water utilized was processed through a Milli-Q water purification system provided by Millipore, based in Bedford, MA, USA. The antibodies for GAPDH, PI3K, AKT, mTOR, and ES were acquired from Cell Signaling Technology, located in Boston, USA. Additionally, antibodies for IL1R1, CD39, CD73, and CCR6 were obtained from Bosterbio in Wuhan, China. The PV-6000 immunohistochemistry kit was sourced from ZSGB-BIO in Beijing, China. Furthermore, several kits for cytokine detection were procured from Nanjing Jiancheng Biotechnology Co., Ltd. based in Nanjing, China.

2.2. LC–MS identification of chemical components in SSD

The LC–MS/MS analysis was carried out on an Orbitrap Exploris 120 mass spectrometer (Thermo), which was connected to a UHPLC system (Vanquish, Thermo Fisher Scientific). This setup included a UPLC HSS T3 column measuring 2.1 mm by 100 mm, with a particle size of 1.8 μm [19]. The composition of the mobile phase included 5 mmol/L of both ammonium acetate and acetic acid dissolved in water (solution A), along with acetonitrile (solution B). The temperature within the autosampler was maintained at 4 °C, with each sample injection amounting to 2 μL. Analysis was conducted using an Orbitrap Exploris 120 mass spectrometer, recognized for its capacity to capture MS/MS spectra via information-dependent acquisition (IDA) mode, all regulated by the Xcalibur software from Thermo. In this configuration, the software dedicated to acquisition is programmed to perpetually analyze the entire MS spectrum. Settings for the ESI source included: a sheath gas flow rate set at 50 Arb, an auxiliary gas flow rate of 15 Arb, and a capillary temperature maintained at 320 °C. The resolution for full MS was established at 60,000, with MS/MS resolution at 15,000. The collision energies were set to 10, 30, and 60 in NCE mode, accompanied by a spray voltage of 3.8 kV in the positive mode and −3.4 kV in the negative mode. The raw data, once transformed into mzXML format via the ProteoWizard software, underwent a series of analyses using a bespoke R package that incorporates the XCMS kernel, focusing on the identification, extraction, alignment, and integration of peaks. Following this, the data were aligned with the BPDB (V1.0), a proprietary tandem mass spectrometry database, for the purpose of annotating substances. An algorithmic scoring threshold was established at 0.3.

2.3. In silico prediction of possible targets of SSD for RA

2.3.1. Acquisition of RA disease targets

To identify genes linked to rheumatoid arthritis, we extracted pertinent gene targets from several databases, including GeneCards, OMIM, PharmaGkb, TTD, and DrugBank [20,21]. All the collected RA targets were processed, and duplicate targets were deleted to obtain the required total RA targets.

2.3.2. Constructing protein–protein interaction (PPI) networks

In the study, researchers focused solely on human proteins by selecting '*Homo sapiens*' as the study species. They input the protein targets identified from the 'Drug Disease' dataset into the STRING database [22]; The parameters were strictly defined, setting the minimum interaction score at '0.900′ and concealing free points. The rest of the parameters defaulted, and we conducted a protein interaction analysis to develop the PPI network diagram. We then transferred the gathered data into Cytoscape software, version 3.7.2 [23], using the Network Analyzer plugin to execute topology analysis and identify crucial genes within the PPI network.

2.3.3. GO functional enrichment analysis and KEGG pathway analysis

The chosen targets for drug-disease interaction were loaded into the R programming environment to conduct both GO functional enrichment and KEGG pathway analyses [24]. A *p*-value of less than 0.01 served as the threshold for selection in these analyses.

2.3.4. Molecular docking

To confirm that the chosen primary targets were effective for treating RA with SSD, molecular docking studies were conducted to examine interactions between SSD's active components and the drug targets. ChemBioDraw was used to construct 2D structures, after which the 2D files were imported into ChemBio3D software to generate 3D structures and obtain the most stable molecular conformation [25]. The target protein receptor's three-dimensional form was retrieved from the PDB database and loaded into the PyMol software. All water molecules and minor ligands associated with the target protein were removed, finalizing the receptor's preparation. The protein receptor files were imported into AutoDockTools-1.5.6 software for protein molecule hydrogenation and other processing. The center of the prototype ligand location of the target was defined as the active pair interface pocket site, with a pocket size of 1.0 nm. Other parameters were adjusted as needed to determine the active pocket, which was subsequently docked using AutoDock Vina software [26].

2.4. Grouping of experimental animals

Male C57BL/6J mice, aged between 4 and 6 weeks and weighing 15–20 g, were housed under controlled conditions. The room maintained a temperature range of 22–25 °C and a relative humidity of 50%–60 %, with exposure to natural light cycles. All experimental protocols were conducted in a conventional laboratory setting designed for animal studies. Individuals without abnormalities were observed during the experiment. The animal studies reported in this research received approval from the Laboratory Animal Center at Liaoning University of Traditional Chinese Medicine, under the authorization number 21000042022082. These studies adhered strictly to ethical guidelines for the care and protection of laboratory animals.

Four groups of rats were created for this study: a normal control group (NC, with eight rats), a model control group (MC, also eight rats), a group treated with Sishen Decoction (SSD, eight rats), and a group receiving methotrexate (MTX, eight rats). To induce inflammation and establish an adjuvant arthritis model in all groups except for the NC group, each rat received an injection of complete freund's adjuvant (CFA) into the skin on their right hind foot, using a volume of 0.1 l per animal. On the 10th day, 0.05 m CFA was injected into the tail root to enhance immunity [27]. Treatment was started one month after modeling. The dosage of each group was as follows.

(I) In the NC group, each subject received a daily gavage of 1 mL/100 g of physiological saline.
(II) In the MC group, each subject received a daily gavage of 1 mL/100 g of physiological saline.
(III) SSD group: Sishen Decoction was administered once a day by gavage at a dose of 1 mL/100 g.
(IV) Methotrexate group: MTX tablets were ground into powder, physiological saline was added, and a suspension was prepared (containing 0.5 mg of MTX per ml). administered a daily dose of 1 mL per 100 g via gavage.

After the experiment, the mice were euthanized through cervical dislocation, and the necessary experimental tissues were collected for further analysis.

2.5. Pathological observation of the joint synovium

2.5.1. Observation of the circumference of mouse ankles

Prior to euthanasia, the ankle circumferences from each of the four mouse groups were recorded to determine an average value for six mice in each group. This measurement was used to initially assess the impact of various interventions on rheumatoid arthritis (RA) in these groups [28].

2.5.2. Pathological observation of synovial tissue

Hematoxylin and eosin (HE) were used to stain sections of synovial tissue. The roasted slices were dewaxed with xylene for 5 min until transparent and eluted with gradient ethanol to remove xylene. Following a rinse, the sections were submerged in distilled water and then colored with hematoxylin dye for a duration of 5–10 min. Subsequently, they were briefly dipped in 0.5 % hydrochloric acid alcohol for 10 s to prepare for microscope analysis. The sections were then cleansed and treated with eosin stain for 1–2 min before being sequentially dehydrated using increasing concentrations of ethanol. Afterwards, the sections were cleared by immersing them in xylene on two occasions for roughly 10 min each and were encapsulated with neutral gum. These prepared slides were examined through an optical microscope, and the extent of synovitis was evaluated based on the Krenn scale for synovitis assessment [29].

2.5.3. Immunohistochemical staining of synovial specimens

Paraffin tissue specimens were cut into slices. Subsequently, dewaxing and hydration treatment were carried out, and the slices were immersed in xylene solution. Following a gradient ethanol hydration process, the sections underwent three thorough rinses with distilled water. The antigens in the slices were then retrieved by submerging them in a 10 % solution of citrate buffer. The solution containing the slices was heated under high temperature and pressure until it boiled, maintained for 2 min, and then left to cool naturally before the slices were extracted and rinsed with water. To block non-specific binding, the samples were immersed in a hydrogen peroxide solution for 15 min, subsequently sealing the background. Following a PBS wash, the samples received a specified volume of diluted antibodies, specifically targeting CD39, CD73, CCR6, and IL1R1 at a 1:300 dilution ratio, and were left to incubate at 4 °C overnight. Subsequent to another PBS wash, a calculated volume of pika universal secondary antibody was administered dropwise, followed by a 30-min room temperature incubation. Post another PBS rinse, DAB staining solution was applied dropwise for 3–5 min. Observations were made under a microscope after washing the samples with tap water. To finalize, the sections were treated with hematoxylin for 5 min, dehydrated using a graded alcohol series, clarified with xylene, and encapsulated permanently [30].

2.6. ELISA

To measure the serum concentrations of IL-1, IL-6, IL-10, TNF-α, and VEGF, ELISA kits were utilized. Following the procedure, first allow the kit's reagents to acclimate to ambient temperature (20–25 °C). Next, take out the necessary 96-well plate and dispense 100 μl of both the standard and the diluted samples into the appropriate wells of the plate. After ensuring a gentle agitation to mix thoroughly, let the plate stand at room temperature for 20 min. Subsequently, wash the plate using a plate washer. Finally, apply 100 μl of the serum sample to each well and incubate at 37 °C for 2 h. The protocol commenced with a thorough rinsing of the plate, followed by the addition of 100 μl of HRp-labeled secondary antibody to each well. Subsequently, the plate underwent a 30-min incubation at a temperature of 37 °C. After another cleansing, two color development solutions, labeled A and B, were introduced, with each being administered in a volume of 50 μl. This was done in a light-protected environment, allowing the color to develop over a period of 15 min. To conclude the process, 50 μl of stop solution was dispensed into the plate. The optical density (OD) was then measured at 450 nm via an enzyme-linked immunosorbent assay, facilitating the determination of the sample's concentration using the established curve equation [31].

2.7. qPCR determination of related mRNAs

The sample, weighing between 50 and 100 mg, was gathered using the MiniBEST Universal RNA Extraction Kit and deposited into a mortar. Initially, a modest quantity of liquid nitrogen was introduced, and the sample was rapidly pulverized. Following a brief period for the tissue to soften, an additional small measure of liquid nitrogen was applied before the sample was ground once more. After doing three times, add the lysis solution according to the instructions, gradually centrifuge, extract the supernatant, adsorb, wash, and finally add nuclease free water to elute to obtain the total RNA. To measure the RNA concentration, we utilized a BioDrop nucleic acid protein analyzer. We conducted RNA isolation using the PrimeScript® RT Reagent Kit along with the gDNA Eraser Kit. In the first step of removing genomic DNA, the mixture was prepared by combining 2 μl of 5× gDNA Eraser Buffer, 1 μl of gDNA Eraser, and nuclease-

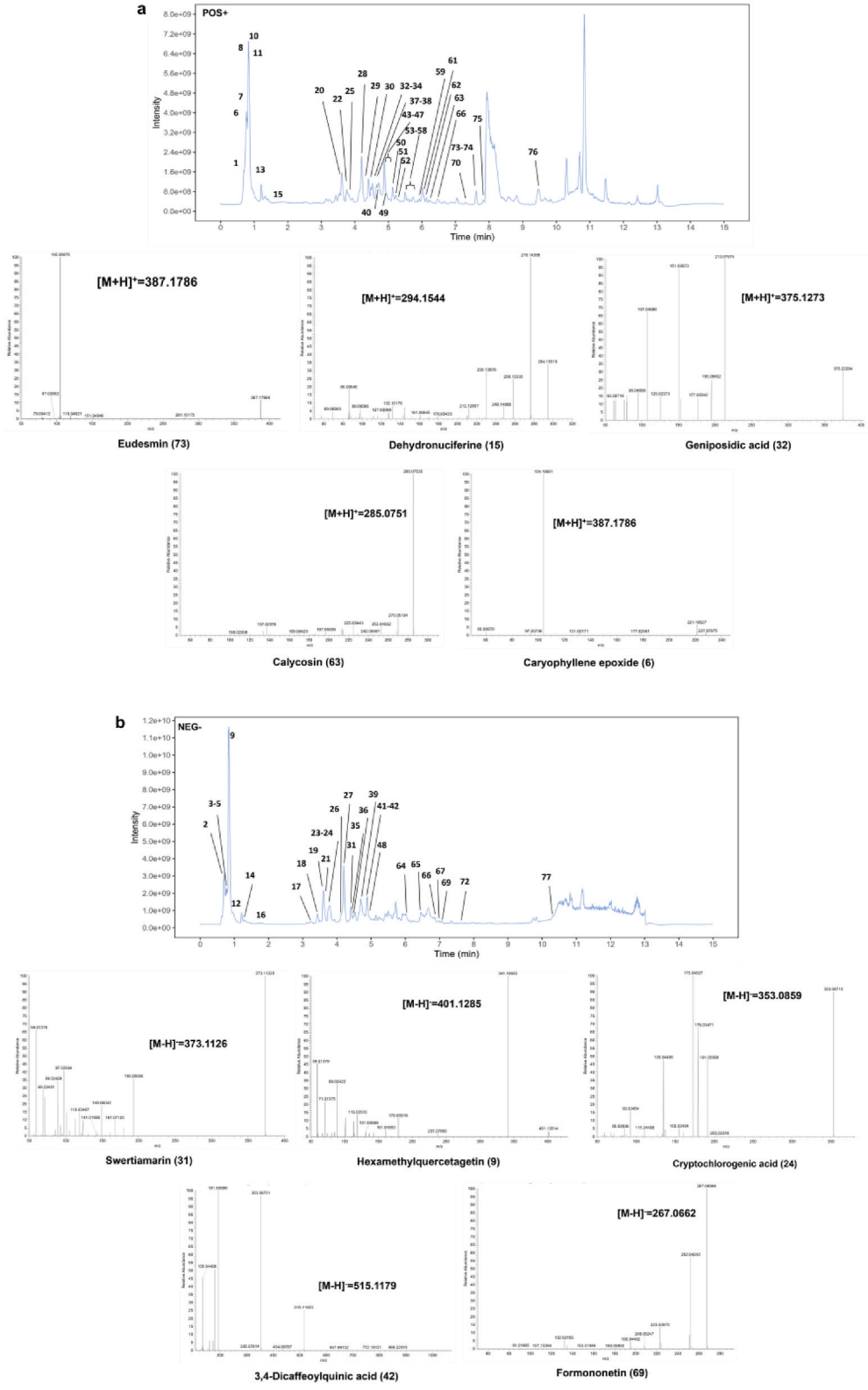

Fig. 1. UPLC-MS analysis of SSD: Total ion chromatogram of SSD in positive model (a)/negative model (b) and ion fragment information of characteristic compounds.

free water with 10 μL of total RNA (0.5 μg). This mixture was incubated at 42 °C for 2 min. Subsequently, to the resultant mix from step one, we added 4 μl of PrimeScript® Buffer 2, 1 μl of PrimeScript® RT Enzyme Mix I, and 4 μl of RNase Free H_2O. The procedure involved maintaining reaction temperatures at 37 °C for 15 min followed by 85 °C for 5 s. Subsequently, the synthesized cDNA was preserved at 4 °C for later applications. Quantitative analysis was conducted using an Mx3000p fluorescence quantitative PCR system

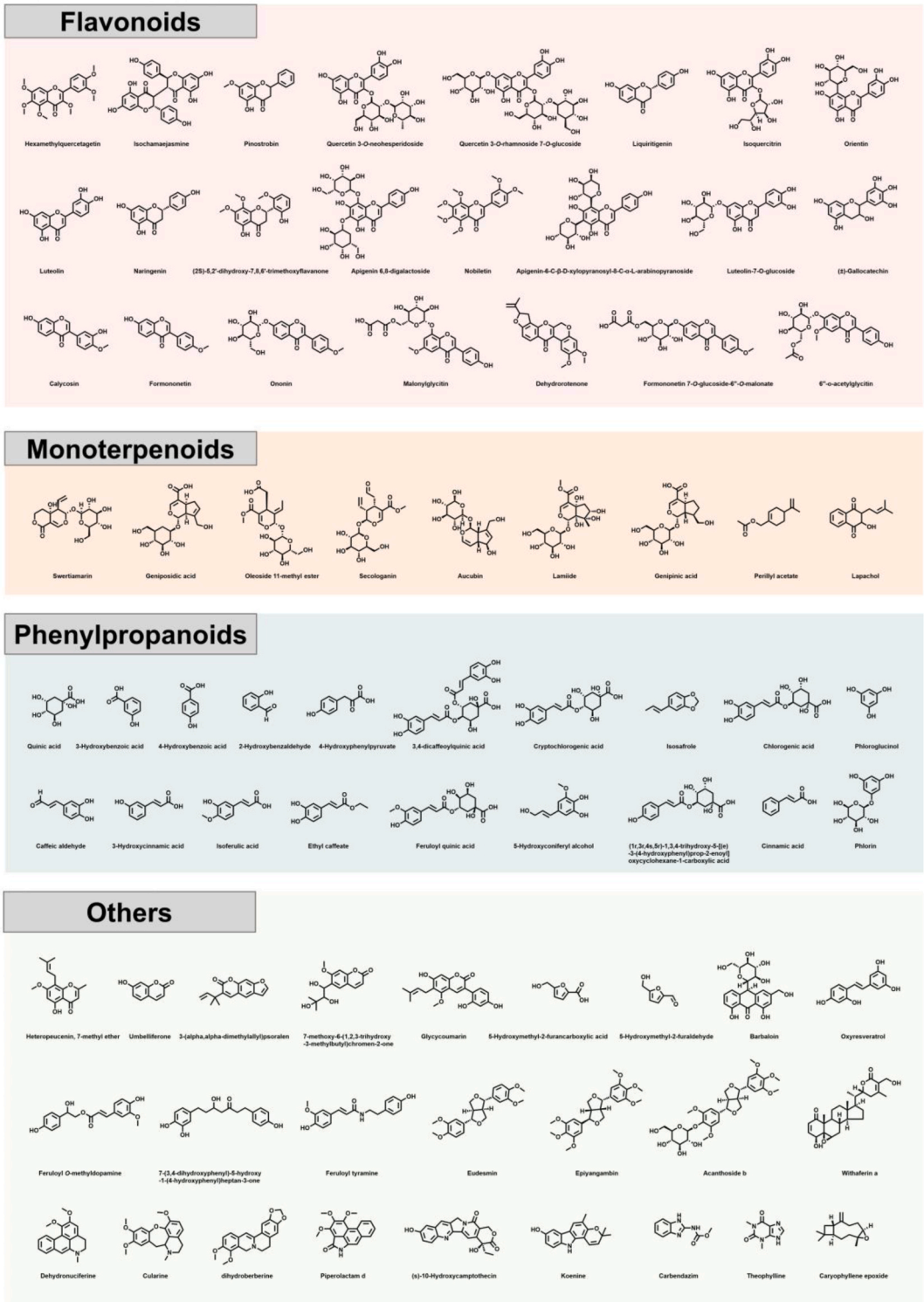

Fig. 2. Identification of the main compounds structure in Sishen Decoction by LC-MS.

from Stratagene (supplied by Agilent Technologies) alongside a TB Green® Premix Ex Taq™ II (TliRNaseH Plus) kit from Takara. The reaction formula included 10 μl of 2 × Master Mix, 5.7 μl of RNase-free water, 0.3 μl of reference fluorescent dye, 1 μl each of upstream and downstream primers, and 2 μl of the reverse-transcribed cDNA. The design of the primers was facilitated using Primer BLAST, with their sequences detailed in the accompanying table [32].

2.8. Western blot analysis of protein expression

In each group, cells were disrupted with 1 mL of RIPA lysis buffer, which included 1 mmol/L PMSF. After SDS–PAGE, a wet transfer membrane was used. The dilution ratio of PI3K, Akt, mTOR, and ES primary antibodies was 1:3000. The membrane, soaked in PBST, was left to incubate at 4 °C overnight before being rinsed three times, with each wash lasting 10 min. The membranes were then incubated with secondary antibodies (dilution ratio 1:5000) and washed with PBST for 10 min for a total of 3 times. The bands were visualized on a chemiluminescence imager using an enhanced chemiluminescence reagent kit (exposure time of 7.0 s) and analyzed using ImageJ software [33].

2.9. Multispectral analysis

2.9.1. Fluorescence quenching analysis

The fluorescence spectrum at 300–500 nm was measured using an RF6000 fluorescence spectrometer (Shimadzu, Japan). AKT solution, at a concentration of 0.1 mg/mL, was treated with SSD solutions, varying in concentration from 0 to 0.6 mg/mL. The combined solutions were then subjected to reactions at temperatures of 298 K, 303 K, and 310 K. Following a stabilization period of 5 min, measurements were performed using an excitation wavelength set at 280 nm and both the excitation and emission bandwidths were maintained at 5 nm each [34].

2.9.2. Fourier transform infrared spectroscopy analysis

Infrared spectroscopy analysis was carried out with a Thermo Nicolet iS50 FTIR spectrometer from Thermo Nicolet Corporation, USA. Both the combined solutions of AKT and SSD and the separate solutions of AKT were prepared for analysis by freeze-drying, followed by examination using the potassium bromide pellet method. We configured the experimental settings to measure wavelengths between 4000 and 400 cm^{-1}, achieving a resolution of 4 cm^{-1} across 32 scans [35]. To prepare the data, we subtracted the background air spectra from each recorded spectrum. The structural analysis of enzymes and complexes was conducted using Thermo OMNIC software (version 8.2, Thermo Fisher Scientific, Inc., USA) and Origin software (version 9.0, Origin Lab, Co., USA).

2.9.3. Circular dichroism analysis

The measurement of circular dichroism (CD) was conducted with a MOS-450 circular dichroism analyzer. The settings for this analysis included a wavelength spectrum of 200–250 nm. During the measurement, the scanning speed was maintained at 60 nm per minute, the spectral resolution and slit width were both set at 1 nm, and the response time was fixed at 1 s. A solution of 0.5 mg/mL SSD and 0.1 mg/mL AKT was prepared in a 1:1 vol ratio for the test sample. For comparison, a control sample containing only 0.1 mg/mL AKT solution was used. Changes in the CD of AKT after SSD treatment were measured. The obtained data were statistically analyzed using CDPro software (Parameters Technology Corporation, USA) to determine the changes in the levels of four components of the protein secondary structure: helix, folding, rotation, and random curling [36].

2.10. Statistical analyses

The statistical analysis was conducted using SPSS 23.0 software, and findings are presented as the mean ± standard deviation. For data that followed a normal distribution and had equal variances, analysis of variance (ANOVA) was employed to determine statistical significance. The Dunnett test was applied for comparisons between paired mean values. The Kruskal-Wallis rank sum test was utilized for data that did not distribute normally. A p-value of less than 0.05 was considered statistically significant.

3. Findings and analysis

3.1. LC–MS identification of the main compounds of SSD

The LC–MS analysis revealed 77 compounds in SSD, which were then cross-referenced with the TCMSP database, including 23 flavonoids, 19 phenolic acids, 9 monoterpenoids and 26 other compounds (alkaloids, lignin, coumarins, etc.) (Figs. 1 and 2 and Table 1). Each of the five Chinese medicines included in SSD is known to possess anti-inflammatory properties. However, their effectiveness in treating RA has not been documented, which could be attributed to the underlying pharmacodynamic substances [37]. In the positive ion mode (Figure a), 30 compounds were identified and 47 compounds were identified in the negative ion mode (Figure b). Among these, several unique compounds were detected for the first time in five traditional Chinese medicines (TCMs). These include 7-methoxy-6-(1,2,3-methylbutyl)chromen-2-one (75), 7-(3,4-dihydroxyphenyl)-5-hydroxy-1-(4-hydroxyphenyl)-3-heptanone (57), isochamaejasmine (7), (2S)-5,2′-dihydroxy-7,8,6′-trimethoxyflavanone (70), apigenin 6-*O*-*β*-glucopyranosyl-8-*O*-*α*-arabinopyranosyl (39), formononetin 7-*O*-glucoside-6″-*O*-malonate (54), oleoside 11-methyl ester (28), (1*R*,3*R*,4*S*,5*R*)-1,3,4-trihydroxy-5-[3-(4-hydroxyphenyl)prop-2-enoyl]oxycyclohexane-1-carboxylic acid (55), and piperolactam D

Table 1
Detailed information on identifying the structure of compounds in Si-Shen-Jian Decoction using LC-MS.

ID	Name	rt	*m/z*	MS fragments	Formula	Class	Type	Peak area
1	Heteropeucenin, 7-methyl ether	6.99	273.11	121.03	$C_{16}H_{18}O_4$	Chromanes	NEG	53462610.36
2	Umbelliferone	4.70	161.02	133.03	$C_9H_6O_3$	Coumarins	NEG	90142123.51
3	3-(alpha,alpha-dimethylallyl)psoralen	0.77	253.09	193.07, 155.00	$C_{16}H_{14}O_3$	Coumarins	NEG	25618940.79
4	7-Methoxy-6-(1,2,3-3-methylbutyl) chromen-2-one	7.92	317.10	287.05	$C_{15}H_{18}O_6$	Coumarins	POS	21486620.68
5	Glycycoumarin	3.76	391.12	211.06, 151.04	$C_{21}H_{20}O_6$	Coumarins	POS	14158202.57
6	5-Hydroxymethyl-2-furancarboxylic acid	0.73	141.02	59.01	$C_6H_6O_4$	Cyclic polyketides	NEG	26227717.13
7	Feruloyl *O*-methyldopamine	6.00	344.15	177.05	$C_{19}H_{21}NO_5$	Diarylheptanoids	POS	16020905.59
8	7-(3,4-Dihydroxyphenyl)-5-hydroxy-1-(4-hydroxyphenyl)-3-heptanone	5.46	369.12	207.06, 175.04	$C_{19}H_{22}O_5$	Diarylheptanoids	POS	11908937.08
9	Feruloyl tyramine	5.92	314.14	177.05, 121.06	$C_{18}H_{19}NO_4$	Diarylheptanoids	POS	10019625.01
10	Hexamethylquercetagetin	0.84	401.13	254.61	$C_{21}H_{22}O_8$	Flavonoids	NEG	896959207.1
11	isochamaejasmine	0.79	543.13	381.08	$C_{30}H_{22}O_{10}$	Flavonoids	POS	46971063.85
12	(±)-Pinostrobin	0.78	269.09	171.01, 89.02	$C_{16}H_{14}O_4$	Flavonoids	NEG	40416889.51
13	Quercetin 3-*O*-neohesperidoside	4.88	609.14	300.03, 271.02	$C_{27}H_{30}O_{16}$	Flavonoids	NEG	36225539.41
14	Quercetin 3-*O*-rhamnoside 7-*O*-glucoside	4.87	611.16	465.10, 303.05	$C_{27}H_{30}O_{16}$	Flavonoids	POS	28302775.02
15	Liquiritigenin	7.61	257.08	242.06	$C_{15}H_{12}O_4$	Flavonoids	POS	26264991.85
16	Isoquercitrin	5.03	465.10	303.05,85.03	$C_{21}H_{20}O_{12}$	Flavonoids	POS	24162407.88
17	Orientin	5.05	449.11	287.05	$C_{21}H_{20}O_{11}$	Flavonoids	POS	20944776.94
18	Luteolin	6.16	285.04	133.03	$C_{15}H_{10}O_6$	Flavonoids	NEG	19291302.59
19	Naringenin	6.44	271.06	151.00, 119.05	$C_{15}H_{12}O_5$	Flavonoids	NEG	16932057.18
20	(2S)-5,2′-Dihydroxy-7,8,6′-trimethoxyflavanone	7.29	347.11	317.07, 289.07	$C_{18}H_{18}O_7$	Flavonoids	POS	16067133.34
21	Apigenin 6,8-digalactoside	4.37	595.16	457.11, 325.07	$C_{27}H_{30}O_{15}$	Flavonoids	POS	13817666.03
22	Nobiletin	7.62	403.14	373.09	$C_{21}H_{22}O_8$	Flavonoids	POS	12197339.68
23	Apigenin 6-c-β-glucopyranosyl-8-c-α-arabinopyranosyl	4.59	563.14	443.10, 353.07	$C_{26}H_{28}O_{14}$	Flavonoids	NEG	11984655.85
24	Luteolin-7-*O*-glucoside	5.23	449.10	287.05	$C_{21}H_{20}O_{11}$	Flavonoids	POS	10062714.37
25	(±)-Gallocatechin	4.10	305.07	225.11, 96.96	$C_{15}H_{14}O_7$	Flavonoids	NEG	10008356.97
26	Calycosin	6.13	285.08	204.05, 125.03	$C_{16}H_{12}O_5$	Isoflavonoids	POS	127172647.4
27	Formononetin	7.06	267.07	186.05	$C_{16}H_{12}O_4$	Isoflavonoids	NEG	71259409.91
28	Ononin	5.67	431.13	269.08	$C_{22}H_{22}O_9$	Isoflavonoids	POS	45217768.38
29	Malonylglycitin	4.71	533.13	285.08	$C_{25}H_{24}O_{13}$	Isoflavonoids	POS	20340411.1
30	Dehydrorotenone	3.29	391.12	229.07, 97.03	$C_{23}H_{20}O_6$	Isoflavonoids	NEG	17388691.94
31	Formononetin 7-*O*-glucoside-6″-*O*-malonate	5.28	517.13	269.08	$C_{25}H_{24}O_{12}$	Isoflavonoids	POS	14756264.74
32	6″-*O*-Acetylglycitin	5.57	489.14	285.08	$C_{24}H_{24}O_{11}$	Isoflavonoids	POS	9535809.4
33	Eudesmin	7.62	387.18	278.06, 131.05	$C_{22}H_{26}O_6$	Lignans	POS	115619787.8
34	Epiyangambin	7.61	445.19	356.96, 297.31	$C_{24}H_{30}O_8$	Lignans	NEG	11149982.72
35	Acanthoside b	5.19	598.25	401.16, 265.11, 205.09	$C_{28}H_{36}O_{13}$	Lignans	POS	10854077.06
36	Swertiamarin	4.20	373.11	204.06, 116.01	$C_{16}H_{22}O_{10}$	Monoterpenoids	NEG	1436301740
37	Geniposidic acid	4.20	375.13	218.03	$C_{16}H_{22}O_{10}$	Monoterpenoids	POS	177353283
38	Oleoside 11-methyl ester	4.11	405.14	243.09, 211.06, 151.04	$C_{17}H_{24}O_{11}$	Monoterpenoids	POS	28943401.12
39	Secologanin	4.89	411.13	249.07	$C_{17}H_{24}O_{10}$	Monoterpenoids	POS	26228255.72
40	Aucubin	4.22	345.12	121.07, 59.01	$C_{15}H_{22}O_9$	Monoterpenoids	NEG	19733214.88
41	Lamiide	3.68	421.13	241.07, 89.02	$C_{17}H_{26}O_{12}$	Monoterpenoids	NEG	12964088.66
42	Genipinic acid	4.11	243.09	211.06, 151.04, 95.05	$C_{11}H_{14}O_6$	Monoterpenoids	POS	10021695.97
43	Perillyl acetate	6.48	195.14	81.07	$C_{12}H_{18}O_2$	Monoterpenoids	POS	9733246.715
44	Lapachol	6.89	241.09	226.06	$C_{15}H_{14}O_3$	Naphthalenes	NEG	10037065.88
45	Quinic acid	3.61	191.06	85.03	$C_7H_{12}O_6$	Phenolic acids	NEG	113849026.5
46	3-Hydroxybenzoic acid	3.92	137.02	93.03	$C_7H_6O_3$	Phenolic acids	NEG	46501263.34
47	4-Hydroxybenzoic acid	4.37	137.02	93.03	$C_7H_6O_3$	Phenolic acids	NEG	44923613.32
48	2-Hydroxybenzaldehyde	1.22	121.03	94.03	$C_7H_6O_2$	Phenolic acids	NEG	18920435.95
49	4-Hydroxyphenylpyruvate	3.79	179.03	135.04	$C_9H_8O_4$	Phenolic acids| Phenolic acids	NEG	10033408.71
50	3,4-Dicaffeoylquinic acid	4.70	515.12	341.04, 207.40	$C_{25}H_{24}O_{12}$	Phenylpropanoids	NEG	520953935.6
51	Cryptochlorogenic acid	3.79	353.09	221.05	$C_{16}H_{18}O_9$	Phenylpropanoids	NEG	388303071.5
52	Isosafrole	9.46	163.08	105.03	$C_{10}H_{10}O_2$	Phenylpropanoids	POS	253544432.7
53	Chlorogenic acid	3.43	353.09	191.06, 179.03, 135.04	$C_{16}H_{18}O_9$	Phenylpropanoids	NEG	253351388.9
54	Caffeate	3.62	163.04	135.04, 89.04	$C_9H_8O_4$	Phenylpropanoids	POS	210967413.4
55	Dicaffeoyl quinic acid	4.70	517.14	499.12, 163.04	$C_{25}H_{24}O_{12}$	Phenylpropanoids	POS	172082555.2
56	Caffeic aldehyde	4.80	165.05	91.05	$C_9H_8O_3$	Phenylpropanoids	POS	136257850.5

(*continued on next page*)

Table 1 (*continued*)

ID	Name	rt	*m/z*	MS fragments	Formula	Class	Type	Peak area
57	3-Hydroxycinnamic acid	4.41	165.05	137.06, 79.05	$C_9H_8O_3$	Phenylpropanoids	POS	107878010.7
58	Isoferulic acid	4.20	195.06	151.04, 95.05	$C_{10}H_{10}O_4$	Phenylpropanoids	POS	91796301.59
59	Ethyl caffeate	4.80	209.08	177.05, 109.03	$C_{11}H_{12}O_4$	Phenylpropanoids	POS	58255425.42
60	Feruloyl quinic acid	4.19	369.12	207.06, 175.04	$C_{17}H_{20}O_9$	Phenylpropanoids	POS	35569426.19
61	5-Hydroxyconiferyl alcohol	3.81	197.08	179.07, 151.08, 109.06	$C_{10}H_{12}O_4$	Phenylpropanoids	POS	17987030.2
62	(1r,3r,4s,5r)-1,3,4-trihydroxy-5-[(e)-3-(4-hydroxyphenyl)prop-2-enoyl] oxycyclohexane-1-carboxylic acid	5.28	339.11	177.05, 145.03	$C_{16}H_{18}O_8$	Phenylpropanoids	POS	10524716.61
63	Cinnamic acid	4.20	149.06	121.06, 103.05	$C_9H_8O_2$	Phenylpropanoids	POS	10062079.81
64	Phlorin	0.84	289.09	127.04	$C_{12}H_{16}O_8$	Phloroglucinols	POS	70413422.57
65	Phloroglucinol	1.21	127.04	109.03	$C_6H_6O_3$	Phloroglucinols| Phloroglucinols	POS	37100554.22
66	Barbaloin	0.93	417.12	341.11, 75.01	$C_{21}H_{22}O_9$	Polycyclic aromatic polyketides	NEG	14983110.99
67	Theophylline	0.77	179.06	161.05, 87.01	$C_7H_8N_4O_2$	Pseudoalkaloids	NEG	242437179.4
68	Caryophyllene epoxide	0.79	221.1856619	128.05	$C_{15}H_{24}O$	Sesquiterpenoids	POS	116881992.9
69	Withaferin a	10.76	469.26	409.24, 214.91	$C_{28}H_{38}O_6$	Steroids	NEG	10364574.68
70	Oxyresveratrol	1.77	243.06	200.06, 110.02	$C_{14}H_{12}O_4$	Stilbenoids	NEG	28529588.56
71	(*s*)-10-Hydroxycamptothecin	0.90	365.11	245.05, 203.05, 185.04	$C_{20}H_{16}N_2O_5$	Tryptophan alkaloids	POS	15255499.11
72	Koenine	0.86	280.14	262.13, 130.09	$C_{18}H_{17}NO_2$	Tryptophan alkaloids	POS	10513685.38
73	Carbendazim	5.35	192.08	160.05	$C_9H_9N_3O_2$	Tryptophan alkaloids	POS	10067573.37
74	Dehydronuciferine	1.76	294.15	129.08	$C_{19}H_{19}NO_2$	Tyrosine alkaloids	POS	102479307.3
75	Cularine	4.71	342.17	297.11, 265.09	$C_{20}H_{23}NO_4$	Tyrosine alkaloids	POS	21454556.43
76	Dihydroberberine	6.01	338.14	184.36, 149.01, 71.05	$C_{20}H_{19}NO_4$	Tyrosine alkaloids	POS	10692940.49
77	Piperolactam d	0.68	296.10	212.06, 146.04	$C_{17}H_{13}NO_4$	Tyrosine alkaloids| Phenanthrenoids	POS	21716161

(1). These findings mark new contributions to the pharmacological profiles of these TCMs. A blend of 23 flavonoids and 19 polyphenols, widely recognized for their anti-inflammatory properties [38,39], indicates that SSD treatment of RA is closely related to its chemical composition. The chemical structure of these first discovered compounds is similar to that of previously reported flavonoids or other polyphenols, and from the structure-activity relationship, it could also be deduced that their effects in reducing inflammation might be comparable, which provides more pharmacodynamic basis for SSD treatment of RA.

As far as we are aware, this research is unprecedented in its comprehensive examination of the primary compounds in SSD, providing a detailed analysis of their structures and potential origins. This could pave the way for pinpointing pharmacodynamically active substances that may be useful in leveraging SSD for clinical use in traditional Chinese medicine.

3.2. Possible targets of SSD treatment for RA based on network pharmacology

Network pharmacology emphasizes the concept of "multitarget and multicomponent therapy", which has the advantages of holistic therapy and may overcome the disadvantages of "single target" [40]. This method sheds light on the intricate relationships between genes, proteins, and metabolites linked to diseases and drugs at the network level, aligning with the comprehensive and systematic perspective of Traditional Chinese Medicine (TCM) theory. As network pharmacology has evolved, the paradigm has shifted from a "single target, single drug" approach to a "network target, multicomponent therapy." The establishment of an interaction network is helpful for further revealing the mutual regulatory relationships between multiple molecules [41]. This approach is commonly applied in the investigation and formulation of traditional Chinese medicine (TCM), particularly in the study of drug pairings and herbal mixtures. It plays a critical role in various aspects of TCM development, including the study of synergistic interactions, forecasting targets for Chinese medicinal compounds, exploring network toxicology within Chinese medicine, identifying bioactive compounds, and examining underlying mechanisms [42,43].

Through the Metascape platform, we identified 349 common targets between drugs and diseases, which were used for Gene Ontology (GO) functional analysis and Kyoto Encyclopedia of Genes and Genomes (KEGG) pathway enrichment analysis. Employing a primary screening criterion of $P < 0.01$, we derived 3904 GO biological function entries. Specifically, Biological Process (BP) 3257 primarily engages in activities such as responding to lipopolysaccharides, reacting to bacterial molecules, and managing cellular chemical stress (Fig. S1).

The study identified 151 cellular components, predominantly associated with areas such as membrane rafts, microdomains, and regions. In terms of Molecular Function (MF), there were 312 items identified, chiefly related to activities like protein tyrosine kinase, transmembrane receptor protein tyrosine kinase, and kinase activity of transmembrane receptor proteins. Additionally, Pathway Analysis (PA) revealed 184 items, with a focus on pathways such as PI3K-AKT, TNF, and HIF-1 signaling pathways (Fig. 3a and Fig. S2).

Analysis of KEGG pathways suggests that SSD could contribute to the management of RA by modulating processes such as inflammation, immunity, and cell cycle progression. SSD's impact on RA involves a variety of biological processes and pathways.

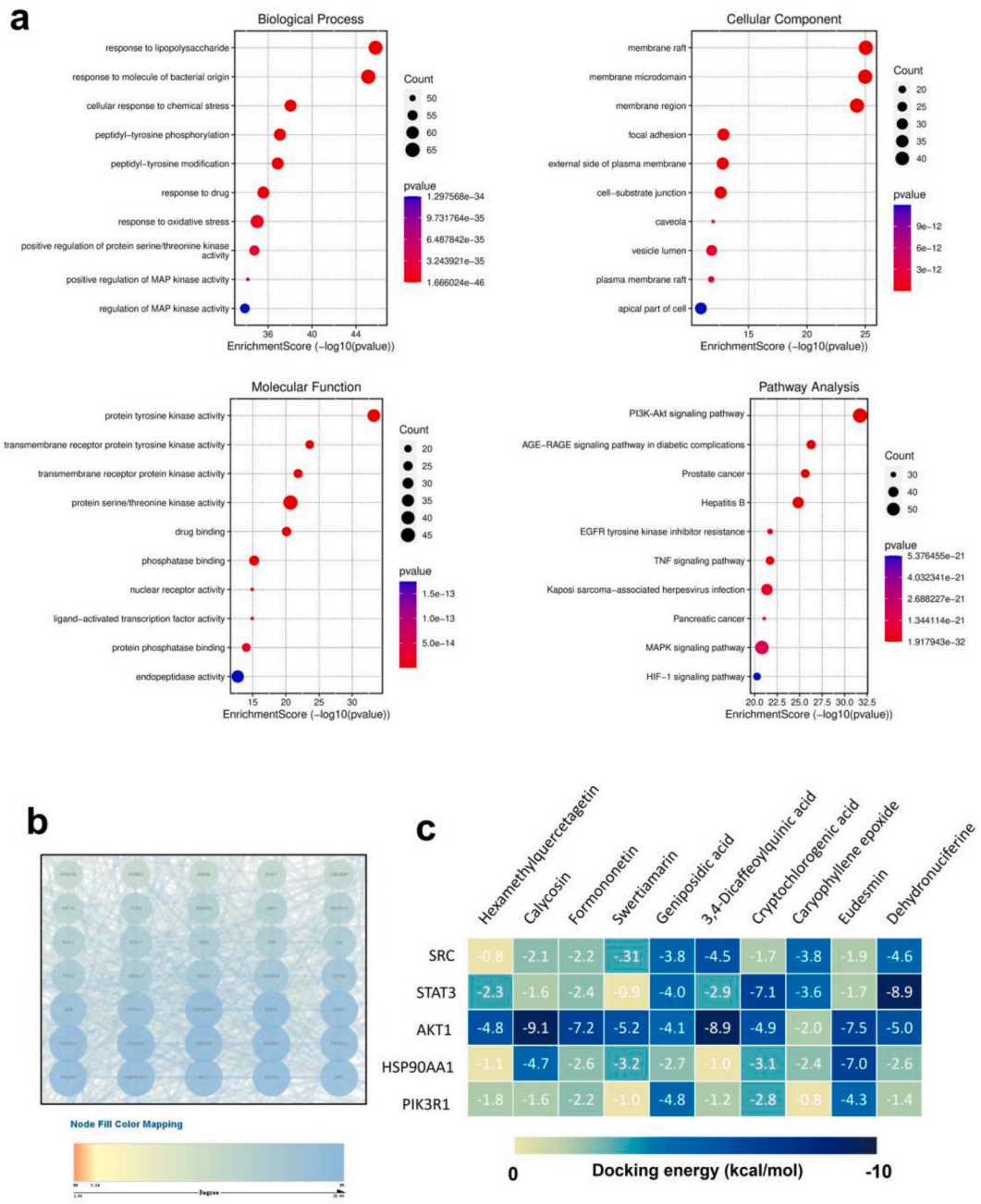

Fig. 3. Gene ontology (GO) analysis for the overlapping target genes of VBF. BP: biological processes; CC: cellular components; MF: molecular functions. Kyoto encyclopedia of genes and genomes (KEGG) pathway analysis for the overlapping target genes of SSD and RA, with the top 10 pathways listed (a). Compound-target network of SSD and RA-most related targets(b). The heatmap represents the minimum docking energies for 5 target proteins and 10 compounds of SSD, with deeper colors indicating stronger binding activity (c).

Within these enhanced pathways, many are recognized as contributing to RA's pathogenesis, notably the PI3K-Akt, TNF, and HIF-1 signaling pathways. Using Cytoscape 3.7.1, a network diagram titled 'Drug Ingredient-Target-Pathway' was created, featuring 230 nodes and 978 connections. The network analyzer tool was employed to evaluate the topology parameters for every element and target within the network. The degree value indicates the count of connections associated with each node. A higher degree value suggests a greater involvement in biological processes. These analyses help identify the key active compounds and central targets of SSD in the treatment of RA. Network topology analysis of the main active ingredients revealed that hexamethylquercetagetin, calycosin, formononetin, swertiamarin, geniposidic acid, 3,4-dicaffeoylquinic acid, cryptochlorogenic acid, caryophyllene epoxide, eudesmin and dehydronuciferine have good correlation degrees, mediality, and proximity centrality. Network topology analysis of the main targets

revealed that SRC, STAT3, AKT1, HSP90AA1 and PIK3R1 were the most likely targets (Fig. 3b and c and Fig. S2).

Therefore, we conducted molecular docking studies on 10 compounds and possible targets (Fig. 3c, Fig. S2 and Fig. S3). According to heatmap analysis of the most stable binding scores, 10 compounds exhibited good binding with AKT. K-AKT signaling pathway information was obtained from the KEGG database. Thus, we hypothesize that the therapeutic effect of SSD in treating rheumatoid arthritis (RA) may be significantly associated with the modulation of the PI3K/AKT signaling pathway, potentially through impacting the phosphorylation of the AKT protein, inhibition of the inflammatory response and induction of cell apoptosis.

3.3. *In vivo effects of SSD treatment on RA*

In the current research, mice models with rheumatoid arthritis (RA) were employed to investigate the treatment potential and underlying mechanisms of SSD in addressing RA. Following the primary immunization, mice treated with SSD exhibited notably less foot swelling compared to those in the control group. In the SSD treatment group, an examination of the synovial tissue revealed improvements such as reduced infiltration of inflammatory cells, less proliferation of the synovial lining layer, and decreased pannus formation, in comparison to the RA model group. Immunochemistry (IHC) methods were employed to assess immune and inflammatory markers associated with RA (CD39, CD73, CCR6, and IL-1R1). The findings showed notable enhancements in these markers in the SSD group relative to the model group.

The cell surface enzymes CD39 and CD73 regulate the production of adenosine by sequentially degrading ATP to AMP and then AMP to adenosine [44]. Treg cells are capable of expressing CD39 and contribute to immune suppression by engaging the adenosine A2AR signaling pathway. Controlling the levels of CD39 and CD73 to reduce the production of adenosine is a crucial strategy for boosting immunity and combating inflammation [45]. This research demonstrated SSD's significant immunomodulatory effect by showing its ability to markedly decrease CD39/CD73 expression in tissues relative to the control group (Fig. 4, $P < 0.05$).

Chemokine receptor 6 (CCR6) is expressed in both lymphoid and nonlymphoid tissues and organs, and its only chemokine ligand is

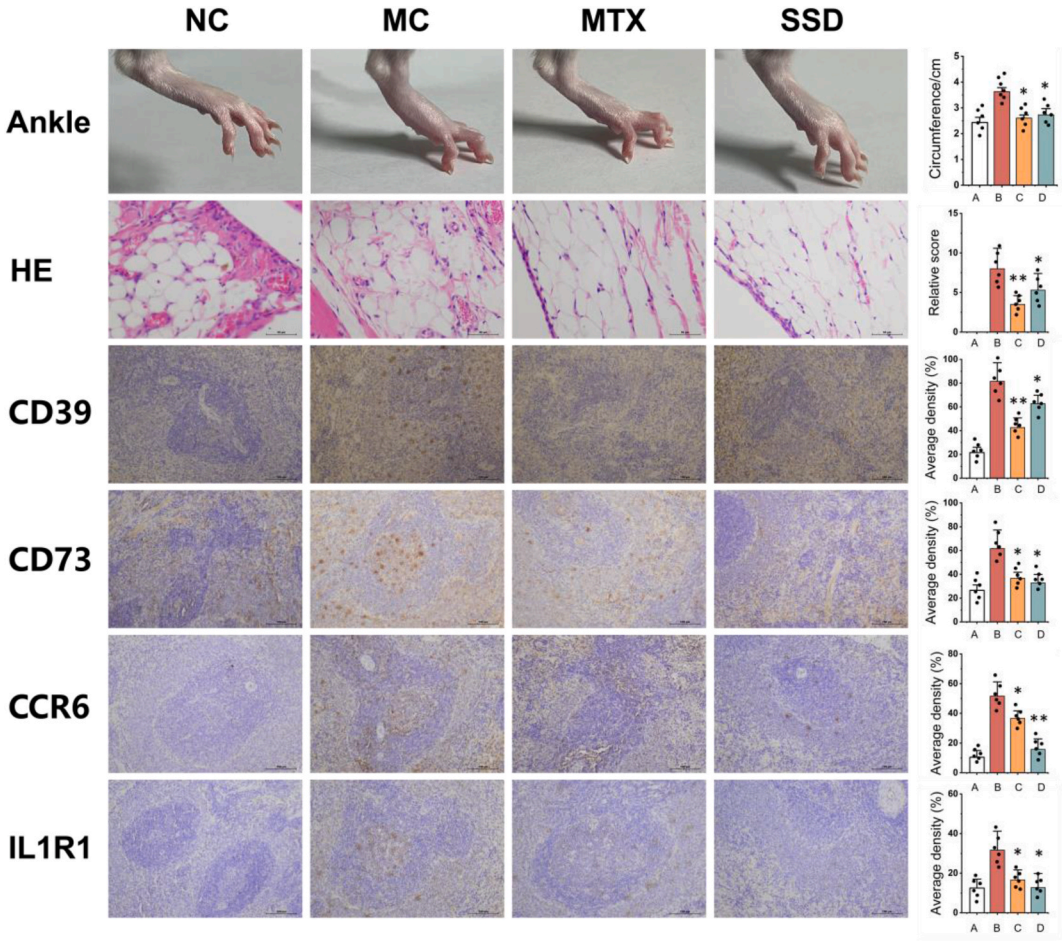

Fig. 4. SSD treatment ameliorated RA rats. Representative images of hind paws from different groups and changes in foot circumference. Hematoxylin eosin staining and immunohistochemical staining (CD31, CD39, CD73, CCR6 and IL1R1) of knee joint synovial slices. $^{*}P < 0.05$, $^{**}P < 0.01$ *vs* Model group.

CCL20 [46]. The combination of the two proteins can cause intracellular actin polymerization and pseudopod formation, thus regulating cell movement and migration. Research indicates CCR6 and associated ligands increase in cancer and inflammatory cells, correlating with tumor metastasis and immune responses [47]. Our findings reveal significantly reduced CCR6 levels in the SSD group compared to the model group (Fig. 4, $P < 0.01$), implying SSD's beneficial impact on inflammation and immunity regulation.

IL1R1 orchestrates immune and inflammatory responses by modulating IL1-triggered signaling cascades, notably NF-κB and MAPK pathways. Upon IL1 binding, IL1R1 activates downstream signals that critically regulate inflammation and immunity [48]. Analysis revealed a marked decrease in IL1R1 expression within the SSD group relative to the model group (Fig. 4, $P < 0.05$). This reduction likely attenuates IL1R1-mediated activation of downstream inflammatory cascades.

SSD reduced serum levels of pro-inflammatory cytokines (TNF-a, IL-6, IL-18, TGF, VEGF) and increased anti-inflammatory IL-10 in RA mice. This suggests SSD mitigates joint inflammation and improves histopathological outcomes in the RA model. Furthermore, SSD exhibited notable upregulation of antioxidant enzymes SOD and CAT, while reducing MDA levels in tissues (Fig. 5a–i), reinforcing its efficacy in alleviating arthritis symptoms in the RA mouse model.

To elucidate SSD's mechanism in RA treatment, we investigated its effects on the PI3K/AKT pathway. Western blotting of knee synovial tissues (Fig. 6a) revealed significantly elevated PI3K, AKT1, and mTOR levels in the model group compared to controls ($P < 0.01$). We also examined ES expression to further understand SSD's impact on this signaling cascade. ES dropped markedly ($P < 0.01$). MTX treatment as primary therapy significantly reduced PI3K ($P < 0.01$), AKT1 ($P < 0.01$), and mTOR ($P < 0.001$) expression, while boosting ES ($P < 0.01$) compared to the model group. SSD, a TCM, also showed notable effects: PI3K, AKT1, and mTOR levels decreased significantly ($P < 0.01$), and ES increased ($P < 0.05$). This data indicates SSD's therapeutic effect on RA, potentially through downregulating PI3K/AKT pathway proteins and upregulating ES expression.

qPCR analysis (Fig. 6b) showed SSD significantly lowered PI3K, AKT, mTOR (all $P < 0.01$), and ES ($P < 0.05$) mRNA levels in knee joint synovial tissue. These PCR and WB findings indicate SSD's ability to downregulate PI3K, AKT, and mTOR mRNA expression in this tissue ($P < 0.01$). SSD inhibits PI3K, AKT, and mTOR expression at both mRNA and protein levels, whereas ES primarily affects protein synthesis. Both modulate the PI3K/AKT pathway. This research corroborates network pharmacology predictions, identifying PI3K/AKT as SSD's probable main target in RA treatment.

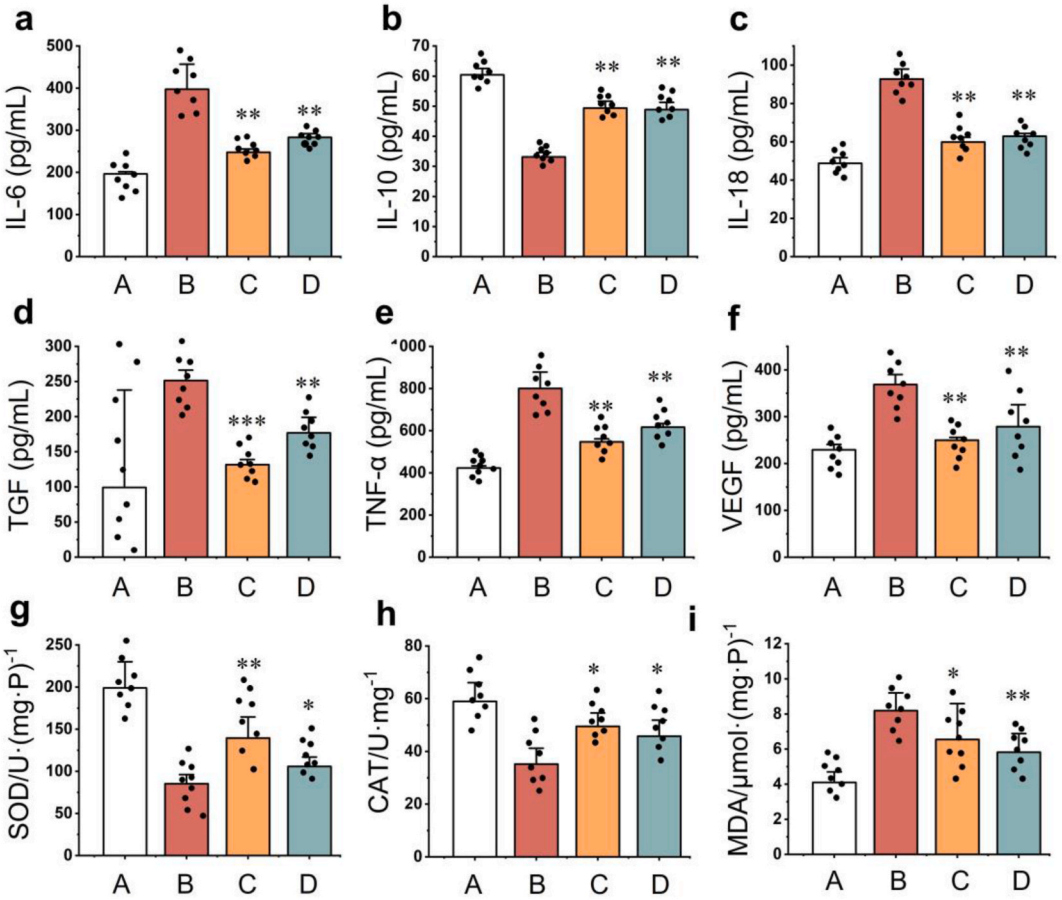

Fig. 5. Comparison of IL-6, IL-10, IL-18, TGF, TNF-α, VEGF in serum (n = 8, x ± s, pg/ml) by ELISA. *$P < 0.05$, **$P < 0.01$, ***$P < 0.001$ *vs* Model group. A: Blank control, B: Model Group, C: methotrexate Group, D: SSD Group.

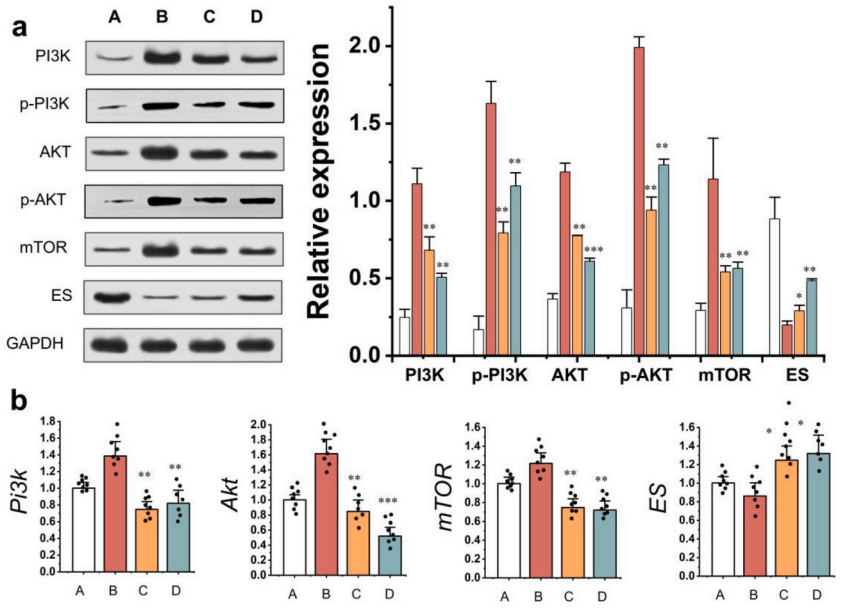

Fig. 6. PI3K/Akt/mTOR pathway-related protein expression levels detected by Western blotting (mean ± SD, n = 3). PI3K/Akt/mTOR pathway-related mRNA expression detected by qPCR (mean ± SD, n = 8). *$P < 0.05$, **$P < 0.01$, ***$P < 0.001$ *vs* Model group. A: Blank control, B: Model Group, C: SSD Group, D: methotrexate Group.

According to network pharmacology, 10 compounds with high concentrations and characteristics of SSD have obvious binding affinities with AKT. Combined with the results of WB and PCR, these findings suggested that the possible target of SSD is AKT. Therefore, further studies of the interaction between SSD and AKT are needed to verify the interaction inference.

3.4. Spectroscopic analysis of the interaction between SSD and AKT

FT-IR has been widely used as an effective method for studying protein conformational changes [49]. Proteins exhibit three distinctive vibrational bands: amide I, II, and III, identifiable through absorption peaks in specific wavenumber ranges. The amide I

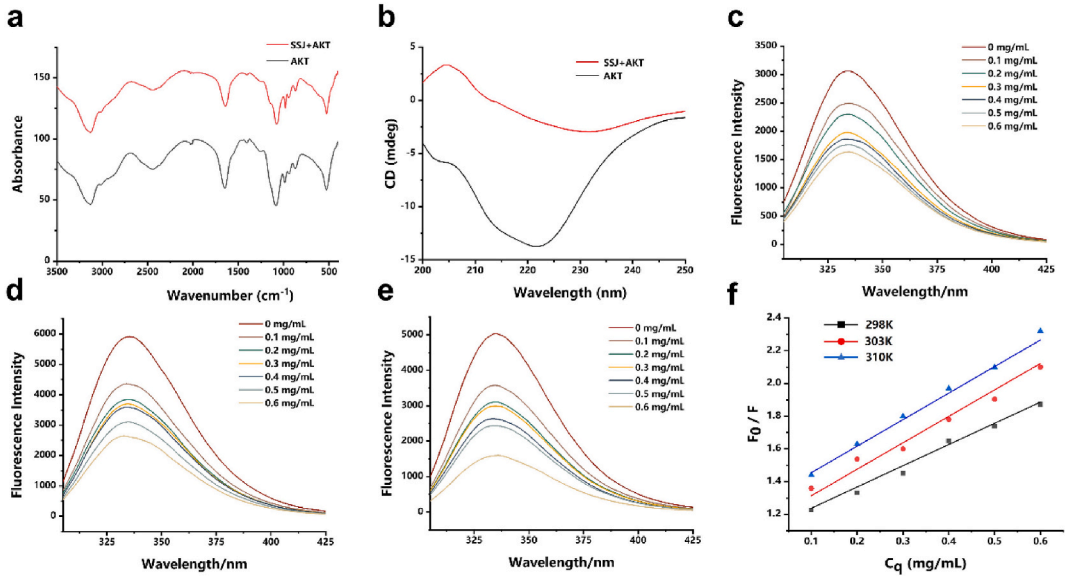

Fig. 7. Interaction mechanism between SSD and AKT. FTIR spectra of AKT treated with SSD (a). CD spectra of AKT treated with SSD (b). Fluorescence spectrum of SSD with AKT at 298 K (c), 303K (d) and 310K (e). Stern−Volmer plots of AKT with the addition of SSD at different temperatures (f).

band, occurring at 1700-1600 cm-1, primarily results from C=O stretching, with minor contributions from N-H bending, C-N stretching, and C-C-N deformation vibrations [50]. This research examined the FT-IR amide I band spectrum of SSD solution with and without AKT. Adding SSD caused the AKT solution's absorption peak to move from 1650 to 1643 cm-1. This shift suggests SSD-AKT interaction altered the peptide's carbonyl hydrogen bonding, modifying AKT's secondary structure (Fig. 7a).

Fig. 7b displays the circular dichroism (CD) data. The CD spectrum of AKT exhibits twin negative bands at 212 nm and 222 nm; these are called helical characteristic bands. The characteristic peaks of AKT are generated by the electron transfer of peptide bonds from n→π* and π→π*. The α-helix content in AKT was 33.6 %. After interaction with SSD, the α-helix content decreased to 32 %, the β-folding and turning angle increased from 11.3 % to 14.3 %, from 21.8 % to 23.1 %, and irregular curling increased from 33.3 % to 35.7 %, respectively. These changes may be due to the expansion of AKT polypeptide chains when SSD binds to AKT amino acid residues, resulting in the loss of the protein hydrogen bond network structure, thereby altering the secondary structure of AKT and facilitating interactions between the two proteins.

The proteins contained three fluorescent chromophores: Trp, Tyr, and Phe. Changes in fluorescence peaks and signals can reflect interactions between substances. AKT has a strong fluorescence emission peak at 335 nm [51]. With the addition of SSD, the fluorescence intensity gradually decreases, and the maximum emission peak position undergoes a blueshift, indicating an interaction between SSD and AKT. Subsequently, quenching at different temperatures was studied, and the Ksv values calculated after fluorescence quenching of AKT by SSD decreased with increasing temperature (Fig. 7c–f). Static quenching played a dominant role in the fluorescence quenching process. AKT's self-phosphorylation is significantly influenced by alterations in its secondary structure. Current understanding suggests that following AKT activation, especially Akt phosphorylates downstream target proteins, the main possible outcomes may be to promote cell survival, growth in size, and proliferation [52]. In this study, WB proved that SSD can effectively regulate the expression of p-AKT protein, which may be caused by changing its secondary structure to promote phosphorylation. However, the further mechanism needs to be confirmed by further molecular interaction experiments.

4. Conclusion

In this research, LC–MS techniques were employed to determine the primary chemical constituents of SSD, revealing 78 different compounds. These include 23 flavonoids, 19 phenolic acids, 9 monoterpenoids, and 26 additional compounds. Employing various approaches like network pharmacology, molecular docking, and experiments using model mice, preliminary findings suggest that SSD primarily targets the PI3K/AKT/mTOR pathway to treat RA. Analyses involving network pharmacology and molecular docking indicate that AKT is a principal target in SSD's regulatory impact. Additional multispectral research has verified that the SSD extract binds strongly with AKT. This pioneering study uncovers the molecular basis of SSD's therapeutic benefits in treating RA, employing a combination of pharmacological assessments, multidimensional simulations, and *in vivo* mouse trials. This research lays a solid groundwork for SSD's future use in TCM clinical practices. The target verification of SSD still needs to be further proved, and the clear dose-effect and structure-activity relationship of its pharmacodynamic substances may be further studied.

Data availability statement

The data underlying this article are available in the article and in its online supplementary material.

The authors declare that they have no known competing financial interests or personal relationships that could have appeared to influence the work reported in this paper.

CRediT authorship contribution statement

Mengyao Gao: Writing – review & editing, Writing – original draft, Visualization, Validation, Methodology, Investigation, Data curation, Conceptualization. **Jun Liu:** Formal analysis, Data curation. **Quansheng Li:** Supervision, Software, Methodology. **Yeyu Zhao:** Supervision, Investigation. **Xin Jin:** Methodology, Investigation, Conceptualization. **Xinyi Tang:** Visualization, Validation. **Congxi Li:** Software, Formal analysis. **Mingli Gao:** Resources, Project administration, Funding acquisition.

Declaration of competing interest

The authors declare the following financial interests/personal relationships have no known competing financial interests or personal relationships that could have appeared to influence the work reported in this paper.

Acknowledgments

This work was supported by the Shenyang Science and Technology Plan Public Health Research and Development Special Project (21-174-9-11).

Appendix A. Supplementary data

Supplementary data to this article can be found online at https://doi.org/10.1016/j.heliyon.2024.e37257.

Abbreviations

SSD	SiShen Decoction
MTX	Methotrexate
RA	Rheumatoid arthritis
TCM	Traditional Chinese Medicine
LC–MS	liquid chromatography–mass spectrometry
PPI	protein–protein interaction
GO	Gene Ontology
KEGG	Kyoto Encyclopedia of Genes and Genomes
FT-IR	Fourier Transform Infrared spectroscopy
CD	Circular dichroism
qPCR	Quantitative real-time polymerase chain reaction
WB	Western blotting

References

[1] R. Makkar, A. Sehgal, S. Singh, N. Sharma, R. Rawat, S. Rashid, et al., Current trends in epigenetic, cellular and molecular pathways in management of rheumatoid arthritis, Inflammopharmacology 31 (2023) 1577–1588, https://doi.org/10.1007/s10787-023-01262-5.

[2] A. Murota, Y. Kaneko, K. Yamaoka, T. Takeuchi, Safety of biologic agents in elderly patients with rheumatoid arthritis, J. Rheumatol. 43 (2016) 1984–1988, https://doi.org/10.3899/jrheum.160012.

[3] W. Jing, C. Liu, C. Su, L. Liu, P. Chen, X. Li, et al., Role of reactive oxygen species and mitochondrial damage in rheumatoid arthritis and targeted drugs, Front. Immunol. 14 (2023) 1107670, https://doi.org/10.3389/fimmu.2023.1107670.

[4] P.-L. Xin, L.-F. Jie, Q. Cheng, D.-Y. Bin, C.-W. Dan, Pathogenesis and function of interleukin-35 in rheumatoid arthritis, Front. Pharmacol. 12 (2021) 655114, https://doi.org/10.3389/fphar.2021.655114.

[5] W. Huang, X. Li, C. Huang, Y. Tang, Q. Zhou, W. Chen, LncRNAs and rheumatoid arthritis: from identifying mechanisms to clinical investigation, Front. Immunol. 12 (2022) 807738, https://doi.org/10.3389/fimmu.2021.807738.

[6] S. Bugatti, S. Gandolfo, F. Ciccia, Autoantibody-negative rheumatoid arthritis: still a challenge for the rheumatologist, The Lancet Rheumatology 5 (2023) 743–755, https://doi.org/10.1016/s2665-9913(23)00242-4.

[7] H.-J. Nel, V. Malmström, D.-C. Wraith, R. Thomas, Autoantigens in rheumatoid arthritis and the potential for antigen-specific tolerising immunotherapy, The Lancet Rheumatology 2 (2020) 712–723, https://doi.org/10.1016/s2665-9913(20)30344-1.

[8] S. Zhou, H. Zou, G. Chen, G. Huang, Synthesis and biological activities of chemical drugs for the treatment of rheumatoid arthritis, Top. Curr. Chem. 377 (2019) 28, https://doi.org/10.1007/s41061-019-0252-5.

[9] R.-S. Mohammed, F.-M. Ibrahim, K.-A. Ahmed, Antiarthritic activity of *Physalis peruviana* fruit extract via inhibition of inflammatory mediators: integrated *in vitro, in vivo* and *in silico* study, J. Ethnopharmacol. 321 (2024) 117502, https://doi.org/10.1016/j.jep.2023.117502.

[10] F.-C. Ceballos, E. Chamizo, C. Mata, C. Cubero, J.-J. Sánchez, R. Veroz, Lerena, et al., Pharmacogenetic sex-specific effects of methotrexate response in patients with rheumatoid arthritis, Pharmaceutics 15 (2023) 1661, https://doi.org/10.3390/pharmaceutics15061661.

[11] Y. Huang, X. Jin, J. Liu, W. Wu, H. Wang, Systems pharmacology approach to investigate the mechanism of *Artemisia argyi* in treating rheumatic diseases, Sci. Rep. 12 (2022) 1–9, https://doi.org/10.1038/s41598-022-23635-6.

[12] T. Wang, Z. Wang, W. Qi, G. Jiang, G. Wang, The role, targets and mechanisms of traditional Chinese medicine in regulating the balance of T helper type 17/ regulatory Tcells in rheumatoid arthritis, International Journal of Rheumatic Diseases 26 (2023) 613–624, https://doi.org/10.1111/1756-185x.14560.

[13] X. Li, Q. Tang, F. Meng, Du P-F, W. Chen, INPUT: an intelligent network pharmacology platform unique for traditional Chinese medicine, Comput. Struct. Biotechnol. J. 20 (2022) 1345–1351, https://doi.org/10.1016/j.csbj.2022.03.006.

[14] X. Wang, Y.-B. Zheng, X.-M. Wang, et al., Clinical effect observation of sishen decoction in treatment of knee osteoarthropathy synovitis, China Journal of Traditional Chinese Medicine and Pharmacy 36 (2021) 3045–3048.

[15] Y. Wang, X. Pan, J. Wang, H. Chen, L.M. Chen, Exploration of Simiao-Yongan Decoction on knee osteoarthritis based on network pharmacology and molecular docking, Medicine 102 (2023) 35193, https://doi.org/10.1097/md.0000000000035193.

[16] J. Zheng, Y. Zhao, Q. Qi, M.-L. Gao, J. Yu, Exploring the molecular mechanism of Sishen Decoction in the treatment of rheumatoid arthritis, Ann. Transl. Med. 10 (2022) 977–988, https://doi.org/10.21037/atm-22-3888.

[17] M. Fan, C. Jin, D. Li, Y. Deng, Y. Lin, Y. Chen, et al., Multilevel advances in databases related to systems pharmacology in traditional Chinese medicine: a 60-year review, Front. Pharmacol. 14 (2023) 1289901, https://doi.org/10.3389/fphar.2023.1289901.

[18] F. Li, N. Hu, J. Hu, Clinical observation of Sishen Decoction in the treatment of synovitis of knee joint of the type of Damp-heat stagnates, Guangming Journal of Chinese Medicine 37 (2022) 1783. https://doi:10.3969/i.issn.1003-8914.2022.10.027.

[19] Y. Wang, F. Zhang, X. Li, J. Wang, J. He, X. Wu, et al., Integrated multi-omics techniques and network pharmacology analysis to explore the material basis and mechanism of simiao pill in the treatment of rheumatoid arthritis, ACS Omega 8 (2023) 11138–11150, https://doi.org/10.1021/acsomega.2c07959.

[20] G. Ozkan, F.-B. Sakarya, A. Akdas, et al., Comprehensive LC-MS/MS phenolic profiling of *Arum elongatum* plant and bioaccessibility of phenolics in their infusions, eFood 5 (2023) 124, https://doi.org/10.1002/efd2.124.

[21] M. Chu, T. Gao, X. Zhang, W. Kang, F. Yuan, Z. Cai, et al., Elucidation of potential targets of San-Miao-San in the treatment of osteoarthritis based on Network pharmacology and molecular docking analysis, Evid. base Compl. Alternative Med. (2022) 7663212, https://doi.org/10.1155/2022/7663212.

[22] V. Joy, B-096 Are we truly Choosing Wisely? An Assessment of nonspecific testing, time to diagnosis and costs related to the diagnosis of Rheumatoid Arthritis, Clin. Chem. 69 (2023) 175, https://doi.org/10.1093/clinchem/hvad097.435.

[23] D. Szklarczyk, J.-H. Morris, H. Cook, M. Kuhn, S. Wyder, M. Simonovic, et al., The STRING database in 2017: quality-controlled protein-protein association networks, made broadly accessible, Nucleic Acids Res. 45 (2016) 362–368, https://doi.org/10.1093/nar/gkw937.

[24] X. Qian, L. Zhang, F. Xie, Y. Cheng, D. Cui, Network-based pharmacological study on the mechanism of guishao-liujun decoction in the treatment of gastric cancer, Front. Pharmacol. 13 (2022) 937439, https://doi.org/10.3389/fphar.2022.937439.

[25] G. Chen, Y. Xu, H. Zhang, Wambua Muema Felix, G. Chen, *Gymnema sylvestre* extract ameliorated streptozotocin-induced hyperglycemia in T2DM rats via gut microbiota, Food frontiers 4 (2023) 1426–1439, https://doi.org/10.1002/fft2.238.

[26] S.-L. Niu, Z.-F. Tong, Y. Zhang, et al., Novel protein tyrosine phosphatase 1B inhibitor-geranylated flavonoid from mulberry leaves ameliorates insulin resistance, J. Agric. Food Chem. 68 (2020) 8223–8231, https://doi.org/10.1021/acs.jafc.0c02720.

[27] J.-L. Tian, X. Si, C. Shu, et al., Synergistic effects of combined anthocyanin and metformin treatment for hyperglycemia *in vitro* and *in vivo*, J. Agric. Food Chem. 70 (2022) 1182–1195, https://doi.org/10.1021/acs.jafc.1c07799.

[28] J.-K. Thuo, P.-K. Towett, T.-I. Kanui, K.S.P. Abelson, Effects of dexamethasone and acetylsalicylic acid on inflammation caused by Complete Freund's adjuvant in the naked mole rat (Heterocephalus glaber), Heliyon 82 (2022) 08920, https://doi.org/10.1016/j.heliyon.2022.e08920.
[29] L.-S. Yan, C.-Y. Brian, Y.-W. Wang, et al., Xuelian injection ameliorates complete Freund's adjuvant-induced acute arthritis in rats via inhibiting TLR4 signaling, Heliyon 9 (2023) 21635, https://doi.org/10.1016/j.heliyon.2023.e21635.
[30] J.-L. Tian, X.-J. Liao, Y.-H. Wang, et al., Identification of cyanidin-3-arabinoside extracted from blueberry as a selective protein tyrosine phosphatase 1B inhibitor, J. Agric. Food Chem. 67 (2019) 13624–13634, https://doi.org/10.1021/acs.jafc.9b06155.
[31] J. Yeong, L. Suteja, Y. Simoni, et al., Intratumoral $CD39^{+}CD8^{+}$ T cells predict response to programmed cell death protein-1 or programmed death ligand-1 blockade in patients with NSCLC, J. Thorac. Oncol. 16 (2021) 1349–1358, https://doi.org/10.1016/j.jtho.2021.04.016.
[32] A.-R. Rocío, C.-C. Jorge, V. Vargas, L.-M. Humbertoa, et al., Development of an Enzyme-Linked Immunosorbent Assay (ELISA) as a tool to detect NS1 of dengue virus serotype 2 in female Aedes aegypti eggs for the surveillance of dengue fever transmission, Heliyon 10 (2024) 29329, https://doi.org/10.1016/j.heliyon.2024.e29329.
[33] X. Gu, J. Hou, J. Rao, R. Weng, S. Liu, LncRNA MALAT1 suppresses monocyte-endothelial cell interactions by targeting miR-30b-5p and enhancing ATG5-mediated autophagy, Heliyon 10 (2024) 28882, https://doi.org/10.1016/j.heliyon.2024.e28882.
[34] K. Chen, B. Huang, J. Feng, et al., Nesfatin-1 regulates the phenotype transition of cavernous smooth muscle cells by activating PI3K/AKT/mTOR signaling pathway to improve diabetic erectile dysfunction, Heliyon 10 (2024) 32524, https://doi.org/10.1016/j.heliyon.2024.e32524.
[35] J.-L. Tian, X. Si, Y.-H. Wang, et al., Bioactive flavonoids from *Rubus corchorifolius* inhibit α-glucosidase and α-amylase to improve postprandial hyperglycemia, Food Chem. 341 (2021) 128149, https://doi.org/10.1016/j.foodchem.2020.128149.
[36] X. Lei, X.-P. Wang, J.-R. Cheng, et al., Study on interaction of rutin and ferulic acid with casein, J. Food Sci. Technol. 38 (2020) 73–80, https://doi.org/10.3969/j.issn.2095-6002.2020.02.010.
[37] Z.-H. Zang, J.-L. Tian, S.-R. Chou, et al., Investigation on the interaction mechanisms for stability of preheated whey protein isolate with anthocyanins from blueberry, Int. J. Biol. Macromol. 255 (2024) 127880, https://doi.org/10.1016/j.ijbiomac.2023.127880.
[38] W. Hu, L.-L. Hong, W. Wang, H. Wang, M. Jiang, X. Li, et al., Unveiling the chemical components variation of Sishen formula induced by different prescription ratios by advanced liquid chromatography/mass spectrometry approaches, Arab. J. Chem. 17 (2023) 105512, https://doi.org/10.1016/j.arabjc.2023.105512.
[39] Y.-C. Chung, S.−S. Jeong, A. Lee, C.-H. Jang, C.-S. Kim, Y.-H. Hwang, Isobavachin, a main bioavailable compound in *Psoralea corylifolia*, alleviates lipopolysaccharide-induced inflammatory responses in macrophages and zebrafish by suppressing the MAPK and NF-κB signaling pathways, Journal of Ethnopharmacol 321 (2024) 117501, https://doi.org/10.1016/j.jep.2023.117501.
[40] S. Sivapalan, D. Sankari, A. Veeramuthu, V. Venkatesan, A. Mangalagowri, Evaluation of the anti-inflammatory and antioxidant properties, and the isolation and characterization of a new bioactive compound, 3,4,9-trimethyl-7-propyldecanoic acid, from *Vitex negundo*, J. Ethnopharmacol. 319 (2024) 117314, https://doi.org/10.1016/j.jep.2023.117314.
[41] Z.-X. Liu, L.-L. Yuan, N. Zhang, et al., Phenylpropanoids from the *Nitraria tangutorum* fruit as glycerol phosphate dehydrogenase inhibitors through in vitro, in silico and in vivo studies, Food Biosci. 53 (2023) 102812, https://doi.org/10.1016/j.fbio.2023.102812.
[42] S. He, J. Shi, H. Chai, et al., Mechanisms with network pharmacology approach of Ginsenosides in Alzheimer's disease, Heliyon 10 (2024) 26642, https://doi.org/10.1016/j.heliyon.2024.e26642.
[43] M.-S. Sven, R. Muhammad, Medicinal polypharmacology: exploration and exploitation of the polypharmacolome in modern drug development, Drug Dev. Res. 85 (2023) 22125, https://doi.org/10.1002/ddr.22125.
[44] C. Wu, L. Lu, Application of drug-target prediction technology in network pharmacology of traditional Chinese medicine, China J. Chin. Mater. Med. 41 (2016) 377–382, https://doi.org/10.4268/cjcmm20160303.
[45] J.-L. Dang, Z.J. Xu, A.-P. Xu, et al., Human gingiva-derived mesenchymal stem cells are therapeutic in lupus nephritis through targeting of CD39−CD73 signaling pathway, J. Autoimmun. 113 (2020) 102491, https://doi.org/10.1016/j.jaut.2020.102491.
[46] Y. Zhu, Z. Zhuang, Q. Wu, S. Lin, N. Zhao, Q. Zhang, et al., CD39/CD73/A2a adenosine metabolic pathway: targets for moxibustion in treating DSS-induced ulcerative colitis, Am. J. Chin. Med. 49 (2021) 661–676, https://doi.org/10.1142/s0192415x21500300.
[47] Y.-N. Zhi, P.-P. Zhang, Y. Luo, et al., CXC chemokine receptor type 5 may induce trophoblast dysfunction and participate in the processes of unexplained missed abortion, wherein p-ERK and interleukin-6 may be involved, Heliyon 10 (2024) 31465, https://doi.org/10.1016/j.heliyon.2024.e31465.
[48] A.-Y. Lee, H. Körner, CC chemokine receptor 6 (CCR6) in the pathogenesis of systemic lupus erythematosus, Immunol. Cell Biol. 98 (2020) 845–853, https://doi.org/10.1111/imcb.12375.
[49] Y. Li, Y. Tian, Q. Wang, R. Lin, Y. Zhang, M. Zhang, et al., Main active components of *Ilex rotunda* Thunb. protect against ulcerative colitis by restoring the intestinal mucosal barrier and modulating the cytokine−cytokine interaction pathways, J. Ethnopharmacol. 318 (2024) 116961, https://doi.org/10.1016/j.jep.2023.116961.
[50] B. Haddad, A.-B. Silvia, M.-V. Castillo, et al., Synthesis, NMR, FT-IR, FT-Raman spectra and thermal studies of Choline bis(trifluoromethylsulfonyl)imide Ionic Liquid combined with DFT Calculations, Journal of molecular structure 1308 (2024) 138017, https://doi.org/10.1016/j.molstruc.2024.138017.
[51] F. Zeeshan, M. Tabbassum, L. Jorgensen, N.-J. Medlicott, Attenuated total reflection fourier Transform infrared (ATR FT-IR) spectroscopy as an analytical method to investigate the secondary structure of a model protein embedded in solid lipid matrices, Appl. Spectrosc. 72 (2017) 268–279, https://doi.org/10.1177/0003702817739908.
[52] Z.-H. Zang, J.-L. Tian, S.-R. Chou, et al., Investigation on the interaction mechanisms for stability of preheated whey protein isolate with anthocyanins from blueberry, Int. J. Biol. Macromol. 255 (2024) 127880, https://doi.org/10.1016/j.ijbiomac.2023.127880.